

Original Article

Quantitative assessment and qualitative assessment for the characteristics of a virtual monoenergetic image in a NAFLD rabbit model: A preliminary study

Ping-Gui Lei^{1*}, Jing Liu^{1*}, Fan Yang^{2*}, Zhu Gong^{1*}, Xiao-Lin Wang¹, Jun Jiao¹, Qing-Hong Duan¹, Ping-Xian Wang³

¹Department of Radiology, The Affiliated Hospital of Guizhou Medical University, Guiyang, Guizhou Province, China; Departments of ²Biomedical Engineering, ³Medical Insurance, Guizhou Medical University, Guiyang, Guizhou Province, China. *Equal contributors.

Received April 10, 2018; Accepted December 10, 2018; Epub March 15, 2019; Published March 30, 2019

Abstract: Objective: To qualitatively and quantitatively assess the diagnostic value of dual-energy virtual monoenergetic images for non-alcoholic fatty liver disease (NAFLD) in a rabbit model. Materials and Methods: Twenty-one 8-week-old rabbits were enrolled in this study; 14 rabbits were fed a high-fat, high-cholesterol diet (experimental group), and 7 rabbits were fed a standard diet (control group). All rabbits underwent a dual-energy unenhanced CT scan. Histological stages were categorized as normal, NAFLD, borderline nonalcoholic steatohepatitis (NASH), and NASH. The features of virtual monoenergetic images for the liver parenchyma, the CT value of virtual monoenergetic image curves (MEIC), and the area under MEIC (AUMEIC) for the NAFLD histological features were analyzed by quantitative assessment and qualitative assessment. Results: As for quantitative assessment, the CT attenuation value of normal livers was higher than that of NAFLD livers (all $P < 0.05$), the optimal contrast-to-noise (CNR) and signal-to-noise (SNR) ratios were obtained at 60 keV for the control rabbits or the rabbits fed with high-fat and high-cholesterol for 4 weeks, and the optimal CNR and SNR were calculated at 60 keV and 70 keV, respectively. The AUMEIC was significantly different for normal livers versus NAFLD livers ($P < 0.05$), and the AUMEIC for the histological features of steatosis, inflammation, and fibrosis were also significantly different (all $P < 0.05$). As for qualitative assessment, the subjective image quality at 60 keV and 70 keV both could be available for diagnosis, and the score of the image quality at 60 keV was significantly higher than the score at 70 keV ($P < 0.05$). Conclusions: The feasibility of a monoenergetic image could provide a potentially effective tool for the diagnosis of NAFLD livers from normal livers. The spectral attenuation curve and its AUMEIC of normal and NAFLD livers are different. We recommend monoenergetic images at 60 keV for evaluating the normal or NAFLD livers due to their optimal CNR and SNR.

Keywords: NAFLD, nonalcoholic steatohepatitis, virtual monoenergetic images, dual energy scanning, quantitative assessment, experimental study

Introduction

Nonalcoholic fatty liver disease (NAFLD) is defined as hepatic intracellular deposition of fat droplets ($> 5\%$ triglycerides) in patients without clinically significant alcohol intake, infection or any other liver disease [1-4]. The earliest and most significant histological characteristic of NAFLD is triglyceride accumulation in hepatocytes. Oxidative stress is triggered by hepatic intracellular triglyceride deposition, leading to simple steatosis, liver injury, inflammation, nonalcoholic steatohepatitis (NASH), and finally cirrhosis and hepatocellular carcinoma

[5-12]. NAFLD is a risk factor for cardiovascular morbidity and for metabolic disease, including type-2 diabetes [13-17]. Therefore, early diagnosis of NAFLD and accurate quantification of liver histological features are valuable in clinical practice.

At present, there are no specific serum biomarkers for the evaluation of the hepatic histology of NAFLD. Aminotransferases are not sensitive or specific enough for the detection of liver fat content. Liver biopsy is the gold standard for the evaluation of NAFLD. However, liver biopsy is not widely available because of its

Virtual monoenergetic image for the evaluation of NAFLD

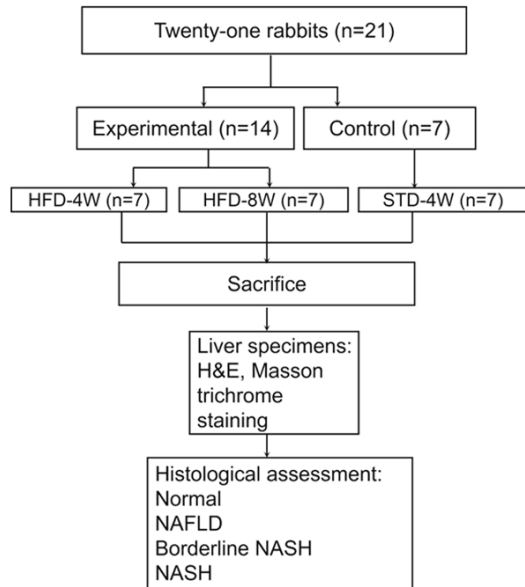


Figure 1. Study design of NAFLD rabbit models. 21 rabbits were randomly classified into a control group (n = 7) or an experimental group (n = 14). All rabbits underwent Dual-energy CT examination. Rabbits in the experimental group were sacrificed either at 4 weeks (n = 7), and 8 weeks (n = 7). All control rabbits underwent dual-energy CT and were sacrificed at 4 weeks. All liver tissue specimens were stained with H&E and Masson trichrome staining. Histological features were classified as follows: normal, NAFLD, borderline NASH, and NASH.

invasiveness. It is critical to find a modality capable of quantifying NAFLD noninvasively.

Traditionally, conventional imaging modalities for NAFLD diagnosis, including ultrasound (US), computed tomography (CT), and magnetic resonance imaging (MRI) have been important, non-invasive modalities for managing patients with NAFLD [18].

Recently, virtual monoenergetic extrapolations from the data of dual-energy CT have been studied, which have the potential to improve the contrast-to-noise ratio (CNR) of contrast-enhanced structures in comparison to a standard single-energy CT examination [19-21]. Compared with traditional CT images, the main benefits of virtual monoenergetic images include less susceptibility to beam hardening artefacts, increased ability to quantify enhancement and more quantitatively accurate attenuation measurements through the construction of spectral curves that delineate tissue attenuation changes at different keV energy levels

[22-24]. Monoenergetic reconstructions generate virtual images at a single energy instead of the conventional poly-energetic CT images [25], which have been utilized in the kidneys, the liver, atherosclerotic carotid artery stenosis, the lungs, et al [26-29]. Currently, however, the characteristics of virtual monoenergetic images for the detection and evaluation of NAFLD histological features have not been identified, and little is known about using this technique for evaluating NAFLD quantitatively and qualitatively.

The purpose of this preliminary study was to qualitatively and quantitatively assess the characteristics of virtual monoenergetic images for diagnosing NAFLD in a rabbit model.

Material and methods

This study was approved by the animal care and use committee of Guizhou Medical University.

The study design for NAFLD rabbit model

Twenty-one New Zealand white rabbits (male = 10, female = 11), 8-weeks-old, were randomly classified into control group (n = 7) and experimental groups (n = 14). The control group was fed a standard diet (STD). The experimental group was fed a high-fat and high-cholesterol diet (HFD, standard diet with an additional 2% cholesterol, 6% yolk powder, 10% lard, and 2% maltose dextrin). All rabbits underwent dual-energy unenhanced CT scans at different time points: Fed with STD or HFD at 4 weeks or 8 weeks. This process was conducted by the Laboratory Animal Research Center of Guizhou Medical University (Guiyang, China). The study design was as follows (**Figure 1**).

Dual-energy CT image acquisition

All the rabbits underwent a dual-energy unenhanced CT scan with a 128-slice MDCT (SOMATOM definition AS+, Siemens, Germany).

For the 80 kVp scan mode, the settings were as follows: tube voltage 80 kVp, tube current 120~130/298 (mAs/ref), collimation 128×0.6 mm, 1 mm slice thickness, 220 mm FOV.

For the 140 kVp scan mode, the settings were: tube voltage 140 kVp, tube current 30~35/71 (mAs/ref), collimation 128×0.6 mm, 1 mm slice

Virtual monoenergetic image for the evaluation of NAFLD

thickness, 220 mm FOV. We obtained all virtual monoenergetic images prior to initiation of the HFD protocol.

Image data analysis

Regions of interest (ROIs) (diameter 0.7 cm-1.0 cm) were placed on the liver parenchyma when the virtual monoenergetic images were available at the Siemens workstation (Syngo CT Workplace VE40B). Virtual monoenergetic images were analyzed by an experienced abdominal radiologist who was blinded to the animal's diet. The radiologist took care to avoid large bile ducts and hepatic vessels on the CT image. One ROI was placed in the left lateral lobe, another one in the left medial lobe, and the third one in the right lobe, and the left hepatic vein and the gallbladder were used as anatomic landmarks. CT attenuation values of each ROI were recorded, the average CT value of three ROIs was calculated for analysis. The CT values of each virtual monoenergetic image were set from 40 keV to 190 keV at the intervals of 10 keV for statistical analysis.

Quantitative assessment

The objective assessment of virtual monoenergetic images includes the CT attenuation of liver parenchyma, the CNR and SNR of virtual monoenergetic images for liver parenchyma, and AUMEIC. Firstly, the CT attenuation measurement was performed for the virtual monoenergetic image at each energy level on the workstation (Syngo CT Workplace VE40B). Three ROIs were conducted in the left lateral lobe, the left medial lobe, and the right lobe by utilizing the left hepatic vein and the gallbladder as anatomic landmarks. The CT attenuation of each ROI was recorded, and the mean CT value was calculated for the analysis. Secondly, the CT values of muscle and air were also measured by placing the ROI on different keV levels on axial images. ROIs (0.7-1.0 cm²) were measured and avoided the lesions, calcification, and artifacts. The standard deviation (SD) of CT attenuation of air at the level of the left hepatic vein about 1 cm distal to the anterior abdominal skin was defined as background noise. Depending on the data of the CT value and SD, CNR and SNR were calculated using the following formulas:

$$CNR_{liver} = \frac{|CT_{liver} - CT_{muscle}|}{SD} \quad (1)$$

$$SNR_{liver} = \frac{CT_{liver}}{SD} \quad (2)$$

Where CT_{liver} is the CT value of liver parenchyma, CT_{muscle} is the CT value of erection muscle, SD is standard deviation (SD) of CT value of air.

Thirdly, the AUMEIC was performed based on the CT value of each level monoenergetic image by the following formula:

$$S_{AUMEIC} = \int_a^b f(x) d(x) \approx \frac{b-a}{n} (\frac{1}{2}y_0 + y_1 + \dots + y_{n-1} + \frac{1}{2}y_n) \quad (3)$$

Where S_{AUMEIC} is the area under the monoenergetic image curve integrated from 40 keV to 190 keV, $f(x)$ is the equation fitting the monoenergetic image curve, $d(x)$ is the differential, a is of 40 keV, b is of 190 keV, y_n is the CT value of liver parenchyma at different keV levels of the monoenergetic image.

Qualitative assessment

With regards to the qualitative assessment, the spectral attenuation curves were available according to various different keV levels of virtual monoenergetic images. The optimal virtual monoenergetic images with the highest CNR and SNR were evaluated by two experienced abdominal radiologists who were blinded to the rabbit's diet with a five-point scale.

The overall Image quality was scored as follows: Score of 1 = poor; Score of 2 = suboptimal; Score of 3 = diagnostic; Score of 4 = superior; Score of 5 = excellent.

Histological analysis

Following dual energy CT examinations, all rabbits were sacrificed under deep anesthesia using a 5 ml potassium chloride injection through the auricular veins. All liver specimens were stained with H&E and Masson staining. The sections were reviewed by an experienced pathologist who was blinded to the rabbit's diet and sacrifice time point. The reference standards were as follows [30].

A NAFLD activity score was assigned to each pathological section: The unweighted sum of steatosis (score 0-3), lobular inflammation (score 0-2), and hepatocellular ballooning (score 0-2).

After the NAFLD activity score was assessed, each study subject was classified into various

Virtual monoenergetic image for the evaluation of NAFLD

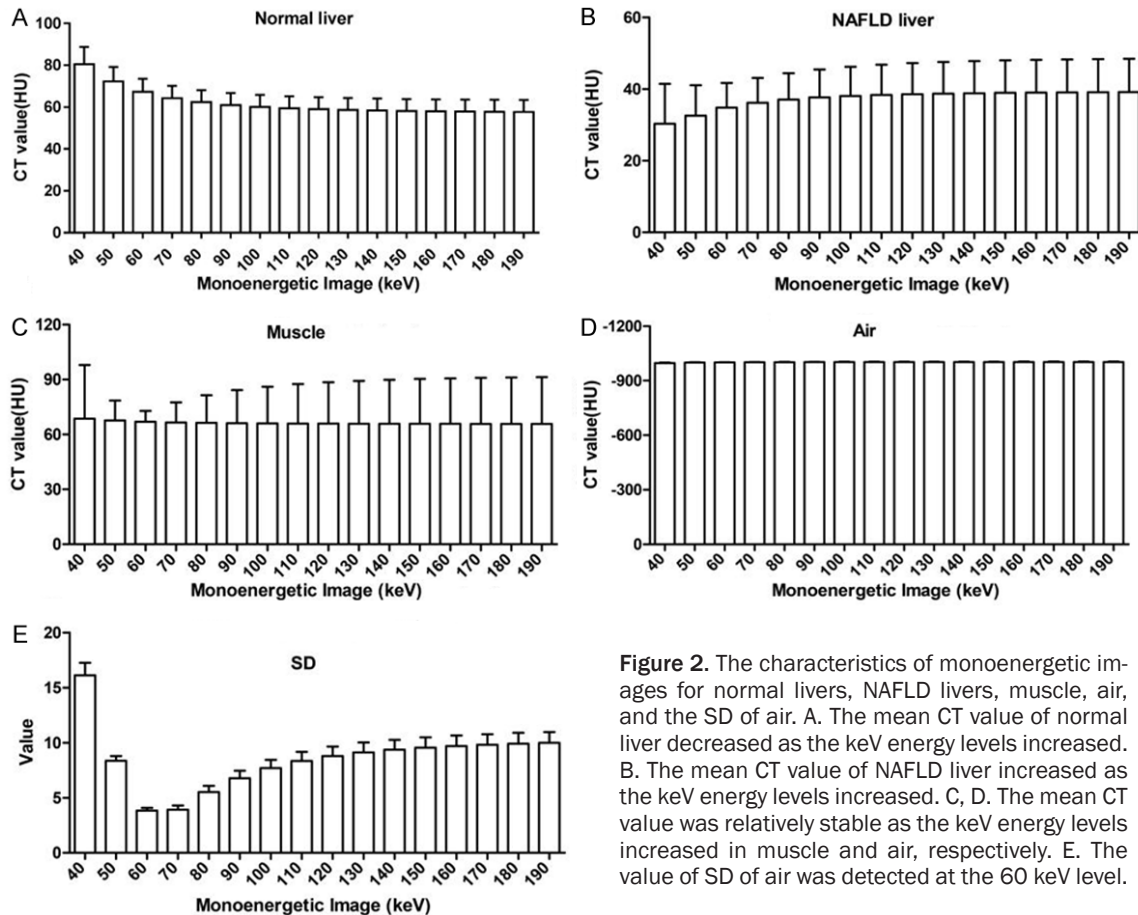


Figure 2. The characteristics of monoenergetic images for normal livers, NAFLD livers, muscle, air, and the SD of air. A. The mean CT value of normal liver decreased as the keV energy levels increased. B. The mean CT value of NAFLD liver increased as the keV energy levels increased. C, D. The mean CT value was relatively stable as the keV energy levels increased in muscle and air, respectively. E. The value of SD of air was detected at the 60 keV level.

NAFLD severity groups: Normal: Activity score = 0; NAFLD: Activity score = 1, 2; Borderline: Activity score = 3, 4; NASH: Activity score \geq 5.

The evaluation of liver fibrosis by Masson trichrome staining [31]: F0 = no fibrosis; F1 = perisinusoidal or periportal fibrosis; F2 = perisinusoidal and periportal fibrosis; F3 = bridging fibrosis (portal-portal, portal-central, or central-central); F4 = cirrhosis.

Statistical analysis

The normality assumption of variables was tested according to the Kolmogorov-Smirnov Z test. The CT values of liver parenchyma, erection muscle, air, and the SD of air at the different keV levels were determined with a nonparametric Friedman's test, as well as the CNR and SNR of liver parenchyma. The AUMEICs of normal, NAFLD, borderline, and NASH were analyzed by one-way ANOVA, the AUMEICs of steatosis and inflammation were also determined by a one-way ANOVA, and the

AUMEICs of ballooning and fibrosis were tested by a two-tailed independent-sample. The score of image quality was tested by a Wilcoxon signed-rank test between 60 keV and 70 keV. Continuous variables were expressed as the mean \pm SD. Statistical analysis was performed on SPSS software (version 23.0, SPSS Inc., Chicago, IL).

A Kappa analysis and percentage agreement were considered to evaluate the qualitative analysis and performed through MedCalc software (MedCalc 15.2.2, Mariakerke, Belgium). The definitions of inter-observer agreement on the basis of k value were as follows: k values less than 0.20 are an indication of poor strength agreement; k values between 0.21~0.40 are an indication of fair strength of agreement; k values between 0.41~0.80 are an indication of moderate strength of agreement; k values between 0.81~1.00 are an indication of very good strength of agreement. $P < 0.05$ was considered a statistically significant difference.

Virtual monoenergetic image for the evaluation of NAFLD

Table 1. The CT value, CNR, and SNR of liver parenchyma for the normal or NAFLD livers at various keV levels

Monoenergetic Image (keV)	Liver CT value			Liver CNR			Liver SNR		
	Con-4W (n = 7)	Exp-4W (n = 7)	Exp-8W (n = 7)	Con-4W (n = 7)	Exp-4W (n = 7)	Exp-8W (n = 7)	Con-4W (n = 7)	Exp-4W (n = 7)	Exp-8W (n = 7)
40	80.50±8.29	36.50±11.97	24.15±6.14	1.91±1.50	2.10±1.69	2.87±2.05	6.63±1.43	2.29±0.71	1.49±0.31
50	72.27±6.94	36.52±9.88	28.62±4.66	2.47±3.03	3.65±1.79	4.71±1.69	10.94±2.53	4.05±0.81	3.41±0.42
60	67.38±6.19	38.28±7.52	31.36±4.42	4.06±6.31	7.04±4.40	9.38±1.91	19.87±6.57	8.69±2.84	8.16±0.64
70	64.32±5.90	39.35±7.75	33.03±4.58	3.47±4.92	6.39±3.95	8.54±2.23	15.35±4.67	8.83±3.43	8.43±0.66
80	62.34±5.82	40.04±8.59	34.12±4.80	2.61±3.38	4.57±2.77	5.78±2.07	11.17±2.91	6.56±2.09	6.18±0.54
90	61.02±5.76	40.49±9.38	34.83±5.00	2.20±2.68	3.77±2.30	4.54±2.06	9.20±2.10	5.49±1.58	5.14±0.48
100	60.13±5.72	40.82±10.00	35.32±5.15	1.98±2.34	3.33±2.02	3.90±2.06	8.16±1.74	4.93±1.34	4.58±0.44
110	59.47±5.72	41.05±10.49	35.68±5.25	1.86±2.16	3.08±1.86	3.54±2.06	7.55±1.50	4.62±1.25	4.27±0.43
120	59.03±5.72	41.23±10.90	35.93±5.34	1.78±2.01	2.93±1.77	3.32±2.08	7.15±1.37	4.42±1.20	4.09±0.40
130	58.67±5.69	41.33±11.14	36.14±5.42	1.75±1.93	2.83±1.72	3.17±2.09	6.89±1.27	4.29±1.17	3.96±0.40
140	58.41±5.70	41.41±11.36	36.27±5.46	1.72±1.88	2.67±1.75	3.09±2.07	6.69±1.20	4.18±1.14	3.87±0.40
150	58.22±5.69	41.52±11.53	36.39±5.51	1.70±1.83	2.69±1.64	3.04±2.03	6.55±1.16	4.11±1.13	3.81±0.39
160	58.01±5.71	41.56±11.66	36.48±5.57	1.68±1.78	2.64±1.61	2.99±2.00	6.43±1.13	4.06±1.12	3.76±0.39
170	57.90±5.71	41.59±11.75	36.55±5.57	1.67±1.76	2.62±1.60	2.97±1.99	6.36±1.10	4.02±1.12	3.72±0.38
180	57.80±5.71	41.63±11.85	36.59±5.59	1.67±1.74	2.59±1.59	2.94±1.98	6.33±1.08	3.98±1.10	3.69±0.38
190	57.73±5.72	41.67±11.92	36.66±5.62	1.67±1.73	2.58±1.60	2.93±1.97	6.30±1.05	3.96±1.09	3.67±0.38
P value	< 0.001	1.000	< 0.001	< 0.001	< 0.001	< 0.001	< 0.001	< 0.001	< 0.001

Note: Con-4W, control group fed a standard diet for 4 weeks; Exp-4W, experimental group fed a standard diet for 4 weeks; Exp-8W, experimental group fed a standard diet for 8 weeks; CNR, contrast-to-noise ratio; SNR, signal-to-noise ratio.

Results

Characteristics of animal NAFLD severity according to histological features

According to the NAFLD activity score, four rabbits were classified as NAFLD, four rabbits were classified as borderline NASH, and six rabbits were classified as NASH. As for the fibrosis assessment, no fibrosis was observed in the normal or NAFLD livers (n = 4), and two of the four borderline livers (2/4) had a score of F1, and five of the six NASH livers (5/6) had a score of F1 (pericellular fibrosis).

Quantitative analysis for virtual monoenergetic images

In the control group fed a standard diet at 4 weeks (Con-4W), the CT value of liver parenchyma was gradually decreased when increasing the monoenergetic keV levels, and the highest and lowest CT attenuations were observed at 40 keV and 190 keV, respectively. However, for the experiment group fed a high-fat and high-cholesterol diet at 4 weeks (Exp-4W) or 8 weeks (Exp-8W), the CT value of liver parenchyma was increased when the monoenergetic keV levels increased, and the highest and lowest CT attenuations were observed at 190 keV and 40 keV, respectively. Significant statistical differences

existed among the different monoenergetic images (40 keV~190 keV) in the control group or the experiment groups (P < 0.001). The highest SD value was observed at 40 keV, and the lowest SD value was measured at 60 keV. The CT value of muscle was gradually decreased when the monoenergetic keV levels increased (range, 68.66 HU~65.74 HU). The CT value of air was gradually increased when the monoenergetic keV levels increased (range, -996.50 HU~-1002.51 HU) (Figure 2).

The lowest image noise (SD) was detected at 60 keV, according to the CT value of liver parenchyma and muscle, the highest CNR and SNR calculated for the control group were both at 60 keV (4.10±6.26 and 19.9±6.66, respectively), as well as for the experiment group fed with high-fat and high-cholesterol at 4 weeks (7.04±4.4 and 8.69±2.84, respectively). The highest CNR and SNR were at 60 keV and 70 keV for the experiment group fed with high-fat and high-cholesterol at 8 weeks (9.38±1.91 and 8.43±0.66, respectively) (Table 1).

Qualitative analysis for virtual monoenergetic images

For the qualitative analysis, the subjective image quality at 60 keV and 70 keV was evaluated by two experienced abdominal radiolo-

Virtual monoenergetic image for the evaluation of NAFLD

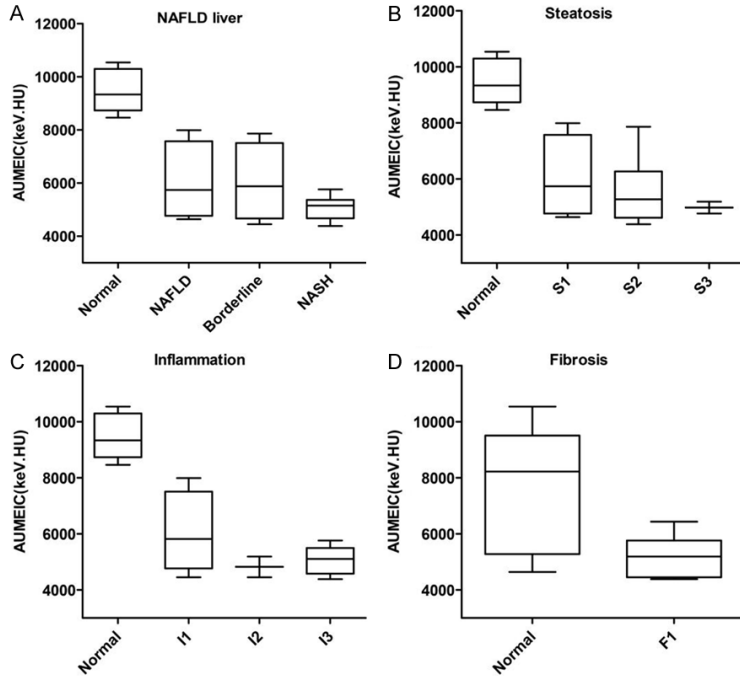


Figure 3. The characteristics of AUMEIC. A. The AUMEIC for NAFLD liver. B-D. The AUMEIC for the histological features of steatosis, inflammation, and fibrosis, respectively.

gists with a five-point scale. The image quality of all the rabbits was proven sufficient to support diagnosis (score ≥ 3). Inter-observer agreement was established between the two experienced radiologists for 60 keV and 70 keV ($k = 0.533$ and $k = 0.323$, respectively). The score of the image quality at 60 keV was higher than the score at 70 keV [(3.29 \pm 0.41) vs. (3.12 \pm 0.27), $P < 0.05$]. The spectral attenuation curves displayed two different types of curves between the normal liver and the NAFLD livers. For the normal livers, the spectral attenuation curve had a tendency to decrease from 40 keV to 190 keV (7/7). For the NAFLD livers, some of the NAFLD livers showed a tendency to decrease (3/14), and the other NAFLD livers had a tendency to increase (11/14).

The characteristics of virtual monoenergetic images for NAFLD livers

The AUMEIC was (9240.92 \pm 866.06) keV.HU for normal livers, (6029.35 \pm 1484.83) keV.HU for NAFLD, (6018.86 \pm 1475.83) keV.HU for borderline NASH, (5076.61 \pm 464.36) keV.HU for NASH. Significant statistical differences existed for normal livers versus NAFLD or higher NAFLD livers ($P < 0.05$). The AUMEICs for the histological features of steatosis, inflammation,

and fibrosis were also significantly different (all $P < 0.05$) (Figure 3).

According to the histological results, the subgroups of NAFLD livers were classified into NAFLD, borderline NASH, and NASH. However, the CT value of liver parenchyma was different as the levels of keV energy in normal, NAFLD, borderline NASH, and NASH livers increased, respectively (Table 2).

Discussion

We detected a significant difference in CT attenuation at different keV levels between the normal livers and the NAFLD livers. The spectral attenuation curves showed a down-sloping for the normal livers, but it showed an up-sloping for most of the NAFLD livers. The AUMEIC of normal livers was larger than that of the NAFLD livers. The optimal CNR and SNR of monoenergetic images for evaluating the image quality of normal or NAFLD livers was found at 60 keV or 70 keV (40 keV-190 keV), and we recommend that 60 keV be used as the optimal monoenergetic image for evaluation of NAFLD livers. The results suggested that monoenergetic images could be available for the quantitative and qualitative assessment of NAFLD livers.

The range of fatty liver disease is often expressed as simple fatty liver to borderline NASH or NASH, with eventual progression to fatty cirrhosis [32, 33]. However, there are exceptions: Some alcoholic fatty livers evolve directly to cirrhosis instead of passing through NASH [32]. We evaluated the NAFLD activity score (NAS) of steatosis, lobular inflammation, and hepatocellular ballooning to classify the severity of NAFLD livers: simply fatty liver (NAS ≤ 2), borderline NASH (NAS = 3 or 4), and NASH (NAS ≥ 5). Four grades of steatosis were observed in NAS as follows [30]: Score of 0 indicated $< 5\%$ liver fat content, score of 1 indicated $5\% \sim 33\%$ liver fat content, score of 2 indicated $> 33\% \sim 66\%$ liver fat content, score of 3 indicated $> 66\%$ liver fat content. Still,

Virtual monoenergetic image for the evaluation of NAFLD

Table 2. The characteristics of liver parenchyma CT values for normal or NAFLD livers at different keV levels

Monoenergetic Image (keV)	Normal (n = 7)	NAFLD (n = 4)	Borderline (n = 4)	NASH (n = 6)	P value
40	80.50±8.29	44.44±5.47	29.88±5.70	21.22±5.22 ^a	< 0.001
50	72.27±6.94	42.60±7.11	31.39±5.91	26.68±3.51 ^a	< 0.001
60	67.38±6.19	41.50±8.34	35.37±4.17	29.99±2.96 ^a	< 0.001
70	64.32±5.90	40.79±9.15	37.82±6.66	32.04±2.91 ^a	< 0.001
80	62.34±5.82	40.35±9.70	39.39±8.73	33.36±3.02 ^a	< 0.001
90	61.02±5.76	40.05±10.04	40.42±10.22	34.23±3.17 ^a	< 0.001
100	60.13±5.72	39.87±10.29	41.14±11.26	34.82±3.26 ^a	< 0.001
110	59.47±5.72	39.72±10.50	41.65±12.00	35.27±3.36 ^a	< 0.001
120	59.03±5.72	39.66±10.72	42.03±12.55	35.57±3.43 ^a	< 0.001
130	58.67±5.69	39.52±10.74	42.30±12.97	35.82±3.49 ^a	< 0.001
140	58.41±5.70	39.47±10.79	42.52±13.28	35.97±3.52 ^a	< 0.001
150	58.22±5.69	39.45±10.85	42.69±13.55	36.14±3.56 ^a	< 0.001
160	58.01±5.71	39.39±10.92	42.82±13.72	36.24±3.60 ^a	< 0.001
170	57.90±5.71	39.36±10.93	42.91±13.84	36.32±3.62 ^a	< 0.001
180	57.80±5.71	39.33±10.97	42.98±14.00	36.38±3.62 ^a	0.001
190	57.73±5.72	39.33±10.99	43.07±14.10	36.46±3.66 ^a	0.001

Note: NAFLD, non-alcoholic fatty liver disease; Borderline, borderline nonalcoholic steatohepatitis; NASH, nonalcoholic steatohepatitis. a, The CT values at different keV levels of monoenergetic image among normal, NAFLD, borderline NASH, and NASH were tested by one-way ANOVA.

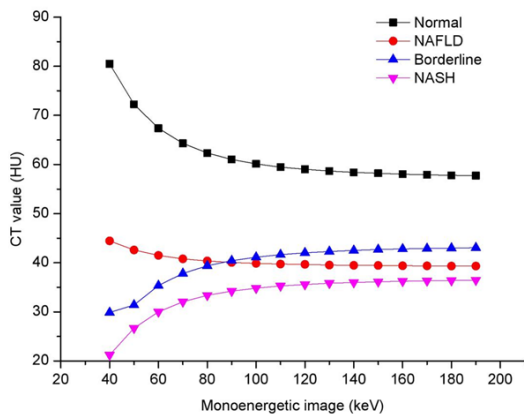


Figure 4. The characteristics of the spectral attenuation curve for the normal liver and the NAFLD subgroups.

significant statistical differences existed for normal liver versus NAFLD or higher NAFLD livers, as well as the AUMEICs for the histological features of steatosis, inflammation, and fibrosis. However, the histological features of steatosis, fibrosis, and inflammation coexisted in the NAFLD liver specimens in our study (7/14). Therefore, it is very difficult to evaluate the differences of CT attenuation or AUMEIC induced only by steatosis, fibrosis, or inflammation, respectively.

The spectral attenuation curve evaluation was different for the normal livers and the NAFLD livers (**Figure 4**). For normal livers, the highest and lowest CT attenuation values were obtained at 40 keV and 190 keV, respectively. The values show a significant attenuation decrease at low energies (approximately 40 keV-100 keV), becoming relatively flat at high energies (approximately 110 keV-190 keV). For the NAFLD livers, the highest CT attenuation value was also observed at 40 keV; however, the slope reduction of a spectral attenuation curve was detected. For borderline NASH or NASH, the highest CT attenuation value existed at 190 keV, and the lowest CT attenuation value was at 40 keV. Two types of spectral attenuation curves were generated by various virtual monoenergetic energy levels, and this phenomenon of different shapes is associated with a relatively high atomic number. One of the benefits of virtual monoenergetic images is quantitatively accurate CT attenuation measurements, which can increase the ability to quantify tissue attenuation changes delineated by construction of spectral curves at various energy levels [23, 24, 34]. X-ray absorption is mainly dependent on two aspects: 1) the photoelectric effect and 2) the atomic number Z of the encountered elements. The photoelectric

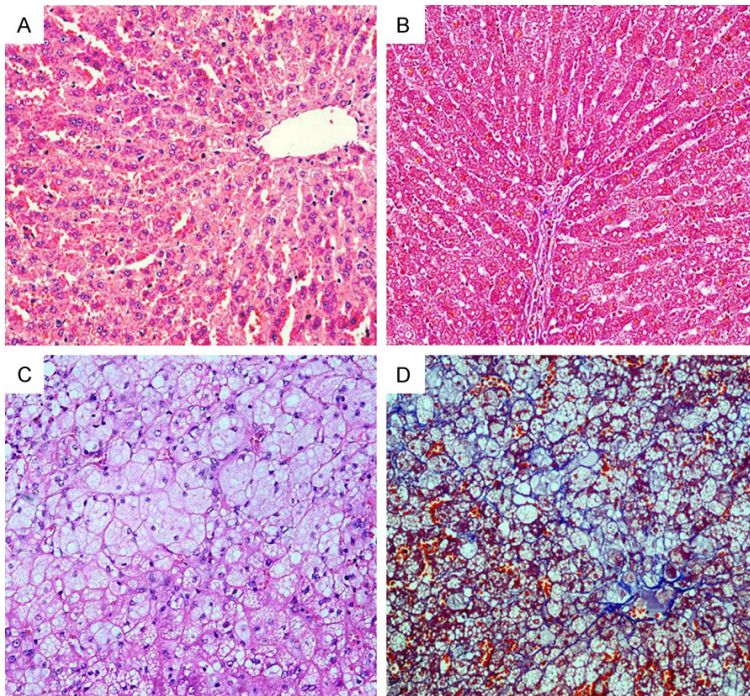


Figure 5. Histological features of the normal liver and F1 in a NASH liver. A, B. Normal liver (H&E, $\times 200$ vs. Masson trichrome, $\times 200$); C. Histological section showing microvesicular steatosis in the hepatocytes (H&E, $\times 200$). D. Photomicrograph of liver specimens showing pericellular fibrosis of F1 (Masson trichrome, $\times 200$).

effect increases strongly as photon energy decreases. Therefore, the attenuation exhibits as increasing significantly at low energies when the elements with a relatively high atomic number Z are encountered [34, 35]. Two different types of spectral attenuation curves were observed in the normal and NAFLD livers, because more hepatic intracellular deposition of fat droplets existed in the NAFLD livers, but not in the normal livers. However, the atomic number Z of fat droplets mainly included carbon ($Z = 6$), hydrogen ($Z = 1$), and oxygen ($Z = 8$), so fat lacks elements with relatively high atomic numbers in the liver.

The spectral attenuation curve had a tendency to decrease from 40 keV to 190 keV and was observed in normal rabbits (7/7), and the spectral attenuation curve had a tendency to increase when increasing the keV energy in the eleven NAFLD rabbits (11/14). However, the AUMEIC was larger than that of any one of the NAFLD rabbits in our study. This suggested that the AUMEIC had the ability to differentiate normal livers from NAFLD or higher severity NAFLD livers.

A monoenergetic image with the optimal CNR and SNR was found at 60 keV in the control rabbits or NAFLD rabbits fed a high-fat and high-cholesterol diet for 4 weeks, and the optimal CNR was found at 60 keV in the NAFLD rabbits fed with a high-fat and high-cholesterol diet for 8 weeks as well. However, the optimal SNR for the NAFLD rabbits fed with high-fat and high-cholesterol for 8 weeks was found at 70 keV. Therefore, monoenergetic images at 60 keV and 70 keV were generated by dual energy CT data to evaluate qualitatively. The subjective image quality of the mono 60 keV images was superior to the subjective image quality of the mono 70 keV images. Therefore, we recommend that monoenergetic images at 60 keV be considered superior for diagnosing normal livers or NAFLD livers. Previous studies showed that

virtual monoenergetic reconstructions of DECT data at 60 keV could significantly improve lesion enhancement and CNR as well as subjective overall image quality [36, 37].

There are some limitations in our study. First, the sample size was small, including the number of subjects in the control group and the experimental group. To further improve the accuracy and diagnostic efficiency of monoenergetic images for evaluating NAFLD livers, the sample size should be increased. Second, patterns of hepatic steatosis can be classified as microvesicular and macrovesicular. Our study showed that the predominant histological feature of rabbit liver specimens with NAFLD is microvesicular steatosis (Figure 5). Previous studies showed that there was a correlation between microvesicular steatosis and NAFLD in the clinical settings [38]. Our study also showed that fibrosis existed in borderline NASH or NASH livers (Figure 5). Third, we used a semiquantitative grading system for evaluating histological features, including steatosis, hepatocellular ballooning, and lobular inflammation. The information about the liver fat content of

compounds was not measured directly in our study, which may better reveal the steatosis of NAFLD livers.

In conclusion, the feasibility of monoenergetic images may prove to provide a potentially effective tool for the differential diagnosis of NAFLD livers. The spectral attenuation curve and its AUMEIC of normal and NAFLD livers are different. Our study showed that the spectral attenuation curve exhibited down-sloping for normal livers and up-sloping for borderline NASH or NASH, and the AUMEIC could provide complementary information to assess those histological features. Last but not least, we recommend using monoenergetic images at 60 keV for evaluating normal or NAFLD livers, and these results should be confirmed clinically in patients with NAFLD in the case of a large sample size.

Acknowledgements

This research was supported by the Joint Fund of Guizhou Department of Science and Technology (LH[2017]7028), the National Natural Science Foundation of China (81760312 and 81660298), and the Guizhou Province Clinical Discipline Subject Fund (2011[52]-03), Doctoral Research Initiation Fund of the Affiliated Hospital of Guizhou Medical University.

Disclosure of conflict of interest

None.

Address correspondence to: Jun Jiao and Xiao-Lin Wang, Department of Radiology, Affiliated Hospital of Guizhou Medical University, Guizhou Medical University, 28 Guiyi Road, Guiyang 550004, Guizhou Province, China. Tel: +86-851-86772193; Fax: +86-851-86855119; E-mail: 1843437663@qq.com (JJ); dr.wang2017@qq.com (XLW)

References

- [1] Blachier M, Leleu H, Peck-Radosavljevic M, Valla DC and Roudot-Thoraval F. The burden of liver disease in Europe: a review of available epidemiological data. *J Hepatol* 2013; 58: 593-608.
- [2] Bedossa P. Current histological classification of NAFLD: strength and limitations. *Hepatol Int* 2013; 7 Suppl 2: 765-770.
- [3] Bedossa P. Histological assessment of NAFLD. *Dig Dis Sci* 2016; 61: 1348-1355.
- [4] Petäjä EM and Yki-Järvinen H. Definitions of normal liver fat and the association of insulin sensitivity with acquired and genetic NAFLD-A systematic review. *Int J Mol Sci* 2016; 17: 633.
- [5] Pais R, Fartoux L, Goumard C, Scatton O, Wendum D, Rosmorduc O and Ratziu V. Temporal trends, clinical patterns and outcomes of NAFLD-related HCC in patients undergoing liver resection over a 20-year period. *Aliment Pharmacol Ther* 2017; 46: 856-863.
- [6] Hatting M and Tacke F. From NAFLD to HCC: is IL-17 the crucial link. *Hepatology* 2017; 65: 739-741.
- [7] Masuzaki R, Karp SJ and Omata M. NAFLD as a risk factor for HCC: new rules of engagement. *Hepatol Int* 2016; 10: 533-534.
- [8] Margini C and Dufour JF. The story of HCC in NAFLD: from epidemiology, across pathogenesis, to prevention and treatment. *Liver Int* 2016; 36: 317-324.
- [9] Cusi K. Role of obesity and lipotoxicity in the development of nonalcoholic steatohepatitis: pathophysiology and clinical implications. *Gastroenterology* 2012; 142: 711-725.
- [10] Younossi ZM, Stepanova M, Rafiq N, Makhlof H, Younoszai Z, Agrawal R and Goodman Z. Pathologic criteria for nonalcoholic steatohepatitis: interprotocol agreement and ability to predict liver-related mortality. *Hepatology* 2011; 53: 1874-1882.
- [11] Adams LA, Lymp JF, St SJ, Sanderson SO, Lindor KD, Feldstein A and Angulo P. The natural history of nonalcoholic fatty liver disease: a population-based cohort study. *Gastroenterology* 2005; 129: 113-121.
- [12] Yatsuji S, Hashimoto E, Tobari M, Taniai M, Tokushige K and Shiratori K. Clinical features and outcomes of cirrhosis due to non-alcoholic steatohepatitis compared with cirrhosis caused by chronic hepatitis C. *J Gastroenterol Hepatol* 2009; 24: 248-254.
- [13] Ballestri S, Nascimbeni F, Baldelli E, Marrazzo A, Romagnoli D and Lonardo A. NAFLD as a sexual dimorphic disease: role of gender and reproductive status in the development and progression of nonalcoholic fatty liver disease and inherent cardiovascular risk. *Adv Ther* 2017; 34: 1291-1326.
- [14] Motamed N, Rabiee B, Poustchi H, Dehestani B, Hemasi GR, Khonsari MR, Maadi M, Saedian FS and Zamani F. Non-alcoholic fatty liver disease (NAFLD) and 10-year risk of cardiovascular diseases. *Clin Res Hepatol Gastroenterol* 2017; 41: 31-38.
- [15] Cusi K, Sanyal AJ, Zhang S, Hartman ML, Bue-Valleskey JM, Hoogwerf BJ and Haupt A. Non-alcoholic fatty liver disease (NAFLD) prevalence and its metabolic associations in patients with type 1 diabetes and type 2 diabetes. *Diabetes Obes Metab* 2017; 19: 1630-1634.

- [16] Scorletti E and Byrne CD. Extrahepatic diseases and NAFLD: the triangular relationship between NAFLD, type 2-diabetes and dysbiosis. *Dig Dis* 2016; 34 Suppl 1: 11-18.
- [17] Lazo M, Bilal U and Perez-Escamilla R. Epidemiology of NAFLD and type 2 diabetes: health disparities among persons of hispanic origin. *Curr Diab Rep* 2015; 15: 116.
- [18] Kinner S, Reeder SB and Yokoo T. Quantitative imaging biomarkers of NAFLD. *Dig Dis Sci* 2016; 61: 1337-1347.
- [19] He J, Ma X, Wang Q, Fan J and Sun Z. Spectral CT demonstration of the superior mesenteric artery: comparison of monochromatic and polychromatic imaging. *Acad Radiol* 2014; 21: 364-368.
- [20] Schneider D, Apfaltrer P, Sudarski S, Nance JW, Haubenreisser H, Fink C, Schoenberg SO and Henzler T. Optimization of kiloelectron volt settings in cerebral and cervical dual-energy CT angiography determined with virtual monoenergetic imaging. *Acad Radiol* 2014; 21: 431-436.
- [21] Sudarski S, Apfaltrer P, Nance JW, Schneider D, Meyer M, Schoenberg SO, Fink C and Henzler T. Optimization of keV-settings in abdominal and lower extremity dual-source dual-energy CT angiography determined with virtual monoenergetic imaging. *Eur J Radiol* 2013; 82: 574-581.
- [22] Yu L, Leng S and McCollough CH. Dual-energy CT-based monochromatic imaging. *AJR Am J Roentgenol* 2012; 199: S9-S15.
- [23] Silva AC, Morse BG, Hara AK, Paden RG, Hongo N and Pavlicek W. Dual-energy (spectral) CT: applications in abdominal imaging. *Radiographics* 2011; 31: 1031-1046.
- [24] Dilmanian FA. Computed tomography with monochromatic x rays. *Am J Physiol Imaging* 1992; 7: 175-193.
- [25] Hardie AD, Picard MM, Camp ER, Perry JD, Suranyi P, De Cecco CN, Schoepf UJ and Wichmann JL. Application of an advanced image-based virtual monoenergetic reconstruction of dual source dual-energy CT data at low keV increases image quality for routine pancreas imaging. *J Comput Assist Tomogr* 2015; 39: 716-720.
- [26] Zopfs D, Lennartz S, Laukamp K, Große HN, Mpotsaris A, Maintz D, Borggrete J and Neuhaus V. Improved depiction of atherosclerotic carotid artery stenosis in virtual monoenergetic reconstructions of venous phase dual-layer computed tomography in comparison to polyenergetic reconstructions. *Eur J Radiol* 2018; 100: 36-42.
- [27] Schabel C, Patel B, Harring S, Duvnjak P, Ramírez-Giraldo JC, Nikolaou K, Nelson RC, Farjat AE and Marin D. Renal lesion characterization with spectral CT: determining the optimal energy for virtual monoenergetic reconstruction. *Radiology* 2018; 287: 874-883.
- [28] De Cecco CN, Caruso D, Schoepf UJ, De Santis D, Muscogiuri G, Albrecht MH, Meinel FG, Wichmann JL, Burchett PF, Varga-Szemes A, Sheafor DH and Hardie AD. A noise-optimized virtual monoenergetic reconstruction algorithm improves the diagnostic accuracy of late hepatic arterial phase dual-energy CT for the detection of hypervascular liver lesions. *Eur Radiol* 2018; 28: 3393-3404.
- [29] Dane B, Patel H, O'Donnell T, Girvin F, Brusca-Augello G, Alpert JB, Niu B, Attia M, Babb J and Ko JP. Image quality on dual-energy CTPA virtual monoenergetic images: quantitative and qualitative assessment. *Acad Radiol* 2018; 25: 1075-1086.
- [30] Kleiner DE, Brunt EM, Van Natta M, Behling C, Contos MJ, Cummings OW, Ferrell LD, Liu YC, Torbenson MS, Unalp-Arida A, Yeh M, McCullough AJ and Sanyal AJ. Design and validation of a histological scoring system for non-alcoholic fatty liver disease. *Hepatology* 2005; 41: 1313-1321.
- [31] Poynard T, Bedossa P and Opolon P. Natural history of liver fibrosis progression in patients with chronic hepatitis C. The OBSVIRC, METAVIR, CLINIVIR, and DOSVIRC groups. *Lancet* 1997; 349: 825-832.
- [32] Diehl AM. Liver disease in alcohol abusers: clinical perspective. *Alcohol* 2002; 27: 7-11.
- [33] Brunt EM. Nonalcoholic steatohepatitis. *Semin Liver Dis* 2004; 24: 3-20.
- [34] Mileto A, Barina A, Marin D, Stinnett SS, Roy CK, Wilson JM and Nelson RC. Virtual monochromatic images from dual-energy multidetector CT: variance in CT numbers from the same lesion between single-source projection-based and dual-source image-based implementations. *Radiology* 2016; 279: 269-277.
- [35] Gabbai M, Leichter I, Mahgerefteh S and Sosna J. Spectral material characterization with dual-energy CT: comparison of commercial and investigative technologies in phantoms. *Acta Radiol* 2015; 56: 960-969.
- [36] Wang XP, Wang B, Hou P, Li R and Gao JB. Screening and comparison of polychromatic and monochromatic image reconstruction of abdominal arterial energy spectrum CT. *J Biol Regul Homeost Agents* 2017; 31: 189-194.
- [37] Wichmann JL, Nöske EM, Kraft J, Burck I, Wagenblast J, Eckardt A, Frellesen C, Kerl JM, Bauer RW, Bodelle B, Lehnert T, Vogl TJ and Schulz B. Virtual monoenergetic dual-energy computed tomography: optimization of kiloelectron volt settings in head and neck cancer. *Invest Radiol* 2014; 49: 735-741.
- [38] Tandra S, Yeh MM, Brunt EM, Vuppalanchi R, Cummings OW, Unalp-Arida A, Wilson LA and Chalasani N. Presence and significance of microvesicular steatosis in nonalcoholic fatty liver disease. *J Hepatol* 2011; 55: 654-659.